

Investigating Cosmological Models and the Hubble Tension using Localized Fast Radio Bursts

JUN-JIE WEI^{1,2} AND FULVIO MELIA³

¹*Purple Mountain Observatory, Chinese Academy of Sciences, Nanjing 210023, China*

²*School of Astronomy and Space Sciences, University of Science and Technology of China, Hefei 230026, China*

³*Department of Physics, The Applied Math Program, and Department of Astronomy, The University of Arizona, AZ 85721, USA*

ABSTRACT

We use the dispersion measure (DM) and redshift measurements of 24 localized fast radio bursts (FRBs) to compare cosmological models and investigate the Hubble tension. Setting a flat prior on the DM contribution from the Milky Way's halo, $DM_{\text{halo}}^{\text{MW}} \in [5, 80] \text{ pc cm}^{-3}$, the best fit for flat Λ CDM is obtained with a Hubble constant $H_0 = 95.8_{-9.2}^{+7.8} \text{ km s}^{-1} \text{ Mpc}^{-1}$ and a median matter density $\Omega_m \approx 0.66$. The best fit for the $R_h = ct$ universe is realized with $H_0 = 94.2_{-6.2}^{+5.6} \text{ km s}^{-1} \text{ Mpc}^{-1}$. We emphasize that the H_0 measurement depends sensitively on the $DM_{\text{halo}}^{\text{MW}}$ prior. Since flat Λ CDM has one more free parameter, $R_h = ct$ is favored by the Bayesian Information Criterion (BIC) with a likelihood of $\sim 73\%$ versus $\sim 27\%$. Through simulations, we find that if the real cosmology is Λ CDM, a sample of $\sim 1,150$ FRBs in the redshift range $0 < z < 3$ would be sufficient to rule out $R_h = ct$ at a 3σ confidence level, while ~ 550 FRBs would be necessary to rule out Λ CDM if the real cosmology is instead $R_h = ct$. The required sample sizes are different, reflecting the fact that the BIC imposes a severe penalty on the model with more free parameters. We further adopt a straightforward method of deriving an upper limit to H_0 , without needing to consider the poorly known probability distribution of the DM contributed by the host galaxy. The theoretical DM contribution from the intergalactic medium (DM_{IGM}) at any z is proportional to H_0 . Thus, requiring the extragalactic DM_{ext} to be larger than DM_{IGM} delimits H_0 to the upside. Assuming flat Λ CDM, we have $H_0 < 89.0 \text{ km s}^{-1} \text{ Mpc}^{-1}$ at a 95% confidence level.

Keywords: Cosmological parameters (339) — Observational cosmology (1146) — Cosmological models (337)
— Radio transient sources (2008)

1. INTRODUCTION

The exact value of the Hubble constant, H_0 , characterizing the current expansion rate of the Universe, is one of the most pressing issues in modern cosmology. In the last decade, the precision of measuring H_0 has been greatly improved, but a significant disparity now appears between its determination at early times and in our local neighbourhood (Verde et al. 2019; Di Valentino et al. 2021). The nearby value of H_0 measured from the Cepheid-calibrated type Ia supernovae (SNe Ia) is $73.04 \pm 1.04 \text{ km s}^{-1} \text{ Mpc}^{-1}$ (Riess et al. 2022), representing a 5σ tension with that inferred from *Planck* cosmic microwave background (CMB) observations in the context of standard Λ CDM ($H_0 = 67.4 \pm 0.5 \text{ km s}^{-1} \text{ Mpc}^{-1}$; Planck Collaboration et al. 2020). If this discrepancy does not arise from unknown systematic uncer-

tainties, new physics beyond Λ CDM may be required to alleviate this so-called ‘Hubble tension’ (Melia 2020; Vagnozzi 2020; Melia 2022). It is therefore essential to find other independent methods of measuring H_0 to investigate this tension more deeply.

Fast radio bursts (FRBs) are mysterious radio transients with excess dispersion measures (DMs) with respect to the expected contributions from the Milky Way (Lorimer et al. 2007; Thornton et al. 2013; Petroff et al. 2019; Platts et al. 2019; Xiao et al. 2021; Zhang 2022). Since the discovery of the first burst (FRB 20010724) in 2007 (Lorimer et al. 2007), more than 600 FRBs have been detected (CHIME/FRB Collaboration et al. 2021). Of these, 26 have been localized, confirming that most, if not all, FRBs originate at cosmological distances.

The DM is the integral over the number density of free electrons along the propagation path between the source and observer, that contains important information on the cosmological distance. Therefore, the combined DM and redshift information of FRBs can be used to study cosmology,

such as constraining the baryon number density of the Universe (Deng & Zhang 2014; McQuinn 2014; Macquart et al. 2020; Yang et al. 2022), the dark energy equation of state (Gao et al. 2014; Zhou et al. 2014; Walters et al. 2018; Wei et al. 2018; Zhang & Li 2020; Zhao et al. 2020; Qiu et al. 2022), cosmic reionization history (Deng & Zhang 2014; Zheng et al. 2014; Hashimoto et al. 2021), cosmic proper distance (Yu & Wang 2017), the baryon mass fraction in the intergalactic medium (IGM; Li et al. 2019, 2020; Walters et al. 2019; Wei et al. 2019; Wang & Wei 2023), the Hubble constant (Hagstotz et al. 2022; James et al. 2022b; Wu et al. 2022), and so on. Additionally, strongly lensed FRBs have also been proposed for probing the nature of compact dark matter (Muñoz et al. 2016; Wang & Wang 2018), for measuring the Hubble constant and cosmic curvature (Li et al. 2018), and for determining the post-Newtonian parameter (Gao et al. 2022).

But though FRBs have previously been used to measure H_0 in Λ CDM (see, e.g., Hagstotz et al. 2022; James et al. 2022b; Wu et al. 2022), they have not yet been utilized for model selection—our primary focus in this paper. Here, we assemble the most up-to-date sample of localized FRBs to examine whether these sources can also be used for comparative studies between competing models, such as Λ CDM and an alternative Friedmann-Lemaître-Robertson-Walker cosmology known as the $R_h = ct$ universe (Melia 2007; Melia & Shevchuk 2012; Melia 2020). In view of the fact that the DM contribution from the FRB host galaxy, DM_{host} , cannot be determined exactly from observations, we further adopt a straightforward method of deriving an upper limit to H_0 by requiring that the IGM portion of the DM, i.e., DM_{IGM} , for any FRB at any z must be smaller than the corresponding extragalactic DM_{ext} , without involving any assumption on the probability distribution for DM_{host} . Our study provides a consistency test of the low-redshift cosmic expansion, and possibly suggests improvements required to arbitrate the Hubble tension.

In Section 2, we briefly describe the DM measurements of localized FRBs, and then constrain the cosmological parameters within the context of Λ CDM and the $R_h = ct$ universe (Section 3). As we shall see, the current FRB sample is not large enough to distinguish these two models, and we forecast in Section 4 how many FRBs will be required from future detections to rule out one or the other expansion scenario at a 3σ confidence level. In Section 5, we introduce the methodology of deriving upper limits on H_0 , followed by the results of our analysis. We end with our conclusions in Section 6.

2. THE PROPERTIES OF LOCALIZED FRBS

The precise localization of an FRB within its host galaxy allows us to correlate its DM_{obs} to a redshift. The DM_{obs} is

a measure of the column density of free electrons, n_e , along the line of sight l : $DM_{\text{obs}} = \int n_e dl / (1+z)$. Physically, we expect DM_{obs} to have contributions from four components: two from the Milky Way, i.e., one from the interstellar medium (ISM) and a second from the halo; and two extragalactic ones, i.e., the IGM and the FRB host galaxy:

$$\begin{aligned} DM_{\text{obs}}(z) &= DM_{\text{MW}} + DM_{\text{ext}}(z) \\ &= DM_{\text{ISM}}^{\text{MW}} + DM_{\text{halo}}^{\text{MW}} + DM_{\text{IGM}}(z) + \frac{DM_{\text{host,loc}}}{1+z}, \end{aligned} \quad (1)$$

where the $(1+z)$ factor converts the local DM contribution from the host galaxy, $DM_{\text{host,loc}}$, to the observed one DM_{host} (Deng & Zhang 2014). The DM due to the Milky Way's ISM, $DM_{\text{ISM}}^{\text{MW}}$, can be estimated quite well using Galactic electron density models (Cordes & Lazio 2002). The contribution from the Milky Way's halo, $DM_{\text{halo}}^{\text{MW}}$, is not as well constrained, but is expected to range from 50 to 80 pc cm^{-3} (Prochaska & Zheng 2019). There are studies suggesting a smaller DM in the Milky Way halo (e.g. Keating & Pen 2020), and also an observation of the M81 FRB 20200110E showing $DM_{\text{halo}}^{\text{MW}} < 32 - 42 \text{ pc cm}^{-3}$ along that line of sight (Kirsten et al. 2022). These values are already rejected by the estimate of Prochaska & Zheng (2019), however. Given the high uncertainty in this term, we shall marginalize $DM_{\text{halo}}^{\text{MW}}$ using a wide flat prior of $[5, 80] \text{ pc cm}^{-3}$. The observed extragalactic dispersion measure, DM_{ext} , can then be derived by deducting the Milky Way's contributions to DM_{obs} , i.e.,

$$\begin{aligned} DM_{\text{ext}} &= DM_{\text{obs}} - DM_{\text{ISM}}^{\text{MW}} - DM_{\text{halo}}^{\text{MW}} \\ &= DM_{\text{IGM}} + DM_{\text{host}}. \end{aligned} \quad (2)$$

Moreover, for a well-localized FRB, the DM_{IGM} value in a certain direction can in principle be measured by subtracting the host galaxy's portion from DM_{ext} , i.e.,

$$DM_{\text{IGM}} = DM_{\text{ext}} - DM_{\text{host}}. \quad (3)$$

The value of DM_{host} is poorly known, however, as it depends very closely on the type of host galaxy, the near-source plasma, and the relative orientations of the host and source (Xu & Han 2015), and may likely range from tens to hundreds of pc cm^{-3} . To model the possible large spread of DM_{host} , we assume that it follows a lognormal distribution with an asymmetric tail to large values (Macquart et al. 2020):

$$P_{\text{host}}(DM_{\text{host}}) = \frac{1}{\sqrt{2\pi}DM_{\text{host}}\sigma_{\text{host}}} \exp \left[-\frac{(\ln DM_{\text{host}} - \mu_{\text{host}})^2}{2\sigma_{\text{host}}^2} \right], \quad (4)$$

where μ_{host} and σ_{host} represent, respectively, the mean and standard deviation of $\ln DM_{\text{host}}$. For the distribution of DM_{host} , the median value and variance are $e^{\mu_{\text{host}}}$ and $e^{(2\mu_{\text{host}} + \sigma_{\text{host}}^2)} [e^{\sigma_{\text{host}}^2} - 1]$, respectively. Using the IllustrisTNG

Table 1. Properties of 26 localized FRBs

Name	Redshift	DM _{obs} (pc cm ⁻³)	DM _{ISM} ^{MW} (pc cm ⁻³)	Repeater	Host Type	Reference
FRB 20200110E	-0.0001	87.75 ± 0.05	30–40	Y	II	Kirsten et al. (2022)
FRB 20181030A	0.0039	103.5 ± 0.3	41	Y	I	Bhardwaj et al. (2021a)
FRB 20180916B	0.0337	348.76 ± 0.1	200	Y	II	Marcote et al. (2020)
FRB 20211127I	0.0469	234.83	42.5	N	III	James et al. (2022b)
FRB 20211212A	0.0715	206	27.1	N	III	James et al. (2022b)
FRB 20201124A	0.098	413.52 ± 0.05	123.2	Y	II	Ravi et al. (2022)
FRB 20190608B	0.1178	338.7 ± 0.5	37.2	N	III	Chittidi et al. (2021)
FRB 20210807D	0.12927	251.9	121.2	N	III	James et al. (2022b)
FRB 20200430A	0.16	380.25 ± 0.4	27	N	III	Heintz et al. (2020)
FRB 20121102A	0.19273	557 ± 2	188	Y	I	Chatterjee et al. (2017)
FRB 20210117A	0.2145	730	34.4	N	III	James et al. (2022b)
FRB 20191001A	0.234	506.92 ± 0.04	44.7	N	III	Heintz et al. (2020)
FRB 20190714A	0.2365	504.13 ± 2	38	N	III	Heintz et al. (2020)
FRB 20190520B	0.241	1205 ± 4	60	Y	I	Niu et al. (2022)
FRB 20191228A	0.2432	297.5 ± 0.05	33	N	III	Bhandari et al. (2022)
FRB 20210320C	0.2797	384.8	42.2	N	III	James et al. (2022b)
FRB 20190102C	0.291	363.6 ± 0.3	57.3	N	III	Bhandari et al. (2020)
FRB 20180924B	0.3214	361.42 ± 0.06	40.5	N	III	Bannister et al. (2019)
FRB 20180301A	0.3304	536 ± 8	152	Y	I	Bhandari et al. (2022)
FRB 20200906A	0.3688	577.8 ± 0.02	36	N	III	Bhandari et al. (2022)
FRB 20190611B	0.378	321.4 ± 0.2	57.8	N	III	Heintz et al. (2020)
FRB 20181112A	0.4755	589.27 ± 0.03	102	N	III	Prochaska et al. (2019)
FRB 20190711A	0.522	593.1 ± 0.4	56.4	Y	I	Heintz et al. (2020)
FRB 20190614D	0.6	959.2 ± 0.5	83.5	N	III	Law et al. (2020)
FRB 20190523A	0.66	760.8 ± 0.6	37	N	III	Ravi et al. (2019)
FRB 20220610A	1.016	1457.624 ± 0.001	31	N	III	Ryder et al. (2022)

simulation, Zhang et al. (2020) derived the DM_{host} distributions for repeating and nonrepeating FRBs at different redshifts. Following Zhang et al. (2020), the localized FRBs are divided into three types based on their host properties: repeating FRBs like FRB 20121102A (type I), repeating FRBs like FRB 20180916B (type II), and nonrepeating FRBs (type III). For each host type, Zhang et al. (2020) found that the median value of DM_{host} (i.e., $e^{\mu_{\text{host}}}$) increases with redshift as $e^{\mu_{\text{host}}(z)} = \kappa(1+z)^\alpha$, where the best-fit values of κ and α are given in their work. In our calculation, we use their results to get μ_{host} and σ_{host} at any redshift of a localized FRB.

In theory, the average value of the IGM portion of DM is related to the cosmological distance scale through (Ioka 2003; Inoue 2004)

$$\langle \text{DM}_{\text{IGM}}(z) \rangle = \frac{3cH_0\Omega_b f_{\text{IGM}}}{8\pi Gm_p} \int_0^z \frac{(1+z')\chi_e(z')}{E(z')} dz', \quad (5)$$

where m_p is the proton mass, H_0 is the Hubble constant, Ω_b is the baryon density parameter, $f_{\text{IGM}} \simeq 0.83$ is the fraction of baryons in the IGM (Fukugita et al. 1998), and $E(z)$ is the dimensionless Hubble parameter that is dependent upon

a given cosmological model. The number of free electrons per baryon is $\chi_e(z) = \frac{3}{4}\chi_{e,\text{H}}(z) + \frac{1}{8}\chi_{e,\text{He}}(z)$, where $\chi_{e,\text{H}}(z)$ and $\chi_{e,\text{He}}(z)$ denote, respectively, the ionization fractions of hydrogen and helium. At redshifts $z \lesssim 3$ hydrogen and helium are fully ionized (Meiksin 2009; Becker et al. 2011), allowing one to set $\chi_{e,\text{H}} = \chi_{e,\text{He}} = 1$, which therefore gives $\chi_e = 7/8$.

It should be emphasized that the actual value of DM_{IGM} would vary significantly around the mean $\langle \text{DM}_{\text{IGM}} \rangle$ due to the large IGM fluctuations. The probability distribution of DM_{IGM} can be derived from numerical simulations of the IGM and galaxy haloes (McQuinn 2014; Prochaska & Zheng 2019), which can be well fitted by the analytic form (Macquart et al. 2020; Zhang et al. 2021)

$$P_{\text{IGM}}(\Delta) = A\Delta^{-\beta} \exp\left[-\frac{(\Delta^{-\alpha} - C_0)^2}{2\alpha^2\sigma_{\text{IGM}}^2}\right], \quad \Delta > 0, \quad (6)$$

where $\Delta \equiv \text{DM}_{\text{IGM}} / \langle \text{DM}_{\text{IGM}} \rangle$, A is a normalization constant, σ_{IGM} is an effective standard deviation, C_0 is chosen such that the mean of the distribution is unity, and α and β are two indices related to the inner density profile of gas in haloes. Following Macquart et al. (2020), we take $\alpha = 3$ and $\beta = 3$. Us-

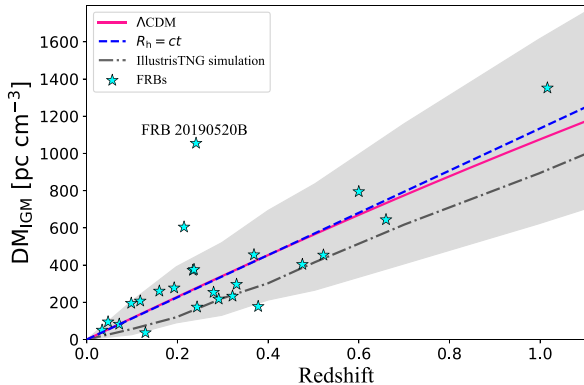


Figure 1. DM–redshift correlation for FRBs. Data points are estimations of the IGM portion DM_{IGM} versus redshift for 24 localized FRBs. The DM_{IGM} values are derived from the observed DM_{obs} after removing the contributions from our Galaxy and the host galaxy. The $DM_{\text{ISM}}^{\text{MW}}$ term is estimated from the Galactic ISM model, and $DM_{\text{halo}}^{\text{MW}}$ and DM_{host} are assumed to be 50 pc cm^{-3} and $50(1+z)^{-1} \text{ pc cm}^{-3}$, respectively. The dot-dashed line represents the DM_{IGM} result deduced from the IllustrisTNG simulation and the gray shaded region encloses the 95% confidence region (Zhang et al. 2021). The other two lines correspond to the predictions of different cosmological models: (solid) flat ΛCDM , with $H_0 = 95.8 \text{ km s}^{-1} \text{ Mpc}^{-1}$ and $\Omega_m = 0.66$; (dashed) the $R_h = ct$ cosmology, with $H_0 = 94.2 \text{ km s}^{-1} \text{ Mpc}^{-1}$.

ing the IllustrisTNG simulation, Zhang et al. (2021) derived realistic distributions of DM_{IGM} at different redshifts. Here we adopt the best-fit values of A , C_0 , and σ_{IGM} for the DM_{IGM} distribution at different redshifts corresponding to their results.

As of today, 26 FRBs have been localized to a host galaxy¹, including 18 apparently non-repeaters and 8 repeaters.² Table 1 lists the redshifts, DM_{obs} (with corresponding uncertainties σ_{obs}), and $DM_{\text{ISM}}^{\text{MW}}$ of all 26 localized FRBs. FRB 20200110E is located in a globular cluster in the nearby galaxy M81, whose distance is only 3.6 Mpc (Bhardwaj et al. 2021b; Kirsten et al. 2022). For such a short distance, the peculiar velocity dominates over the Hubble flow so that it has a negative spectroscopic redshift

¹ Here the terminology of “localized” means the host galaxy has been identified. However, “localized” can also mean that the radio localization is of order arcsec, and different groups have different definitions of how well-localized an FRB has to be to call it “localized” (usually the cutoff is the same as their instrument’s angular resolution). This distinction is important in the context of this work because a given “localization” accuracy (i.e. angular error) is more likely to lead to the identification of the host galaxy for a near-Universe FRB.

² Note that there might be a potential bias from including localized repeating FRBs that have only been localized because they repeat. But as long as the localization is as reliable as any of the others, repeating sources should be fine. Moreover, since the current localized sample size is admittedly small, we use all the FRBs for our analysis.

$z = -0.0001$. Since the DM_{obs} value of FRB 20181030A is only 103.5 pc cm^{-3} (Bhardwaj et al. 2021a), its extragalactic DM_{ext} will be reduced to a negative value after removing $DM_{\text{ISM}}^{\text{MW}}$ and $DM_{\text{halo}}^{\text{MW}}$. That is, the integral upper limit ($DM_{\text{ext}} \equiv DM_{\text{obs}} - DM_{\text{ISM}}^{\text{MW}} - DM_{\text{halo}}^{\text{MW}}$) in the probability of the extragalactic DM_{ext} (see Eq. 8) will become negative. Thus, neither FRB 20200110E nor FRB 20181030A are available for our subsequent maximum likelihood analysis, so we exclude them from the localized FRB sample. Figure 1 shows the estimated DM_{IGM} and measured z values for the remaining 24 FRBs. We have estimated DM_{IGM} by deducting the following contributions from the measured DM_{obs} value: $DM_{\text{ISM}}^{\text{MW}}$ based on the Galactic ISM model; and the assumed $DM_{\text{halo}}^{\text{MW}} = 50 \text{ pc cm}^{-3}$ and $DM_{\text{host}} = 50(1+z)^{-1} \text{ pc cm}^{-3}$. In Figure 1, the dot-dashed line is the DM_{IGM} result estimated from the IllustrisTNG simulation with 95% confidence region (Zhang et al. 2021). FRB 20190520B is associated with a dwarf host galaxy at $z = 0.241$. It was found that FRB 20190520B deviates significantly from the general trend of the $DM_{\text{IGM}}-z$ relation, with an unprecedented DM contribution from its host galaxy (Niu et al. 2022). Since DM_{host} is assumed to follow a lognormal distribution with an asymmetric tail to large values (see Eq. 4), our model ought to be able to account for FRB 20190520B well. Therefore, we do not exclude this FRB from our analysis. In total, there are 24 FRBs for us to consider in the rest of this paper.

3. MODEL SELECTION

We are now in position to use the 24 DM– z measurements of the FRB sample to test and compare certain cosmological models. The cosmological parameters are optimized via a maximization of the joint likelihood function (Macquart et al. 2020):

$$\mathcal{L} = \prod_{i=1}^{24} P_i(DM_{\text{ext},i}), \quad (7)$$

where $P_i(DM_{\text{ext},i})$ is the probability of individual observed DM_{obs} corrected for our Galaxy, i.e., $DM_{\text{ext}} \equiv DM_{\text{obs}} - DM_{\text{ISM}}^{\text{MW}} - DM_{\text{halo}}^{\text{MW}} = DM_{\text{IGM}} + DM_{\text{host}}$. For an FRB at redshift z_i , we have

$$P_i(DM_{\text{ext},i}) = \int_0^{DM_{\text{ext},i}} P_{\text{host}}(DM_{\text{host}}) \times P_{\text{IGM}}(DM_{\text{ext},i} - DM_{\text{host}}) dDM_{\text{host}}, \quad (8)$$

where $P_{\text{host}}(DM_{\text{host}})$ and $P_{\text{IGM}}(DM_{\text{IGM}})$ (see Eqs. 4 and 6) are the probability density functions for DM_{host} and DM_{IGM} , respectively. To determine the model predictions for the average value of $\langle DM_{\text{IGM}}(z) \rangle$ in Equation (5), we need an expression for the model-dependent dimensionless expansion rate $E(z)$. Here we discuss how the fits are obtained for ΛCDM and the $R_h = ct$ universe. It is worth emphasizing that the

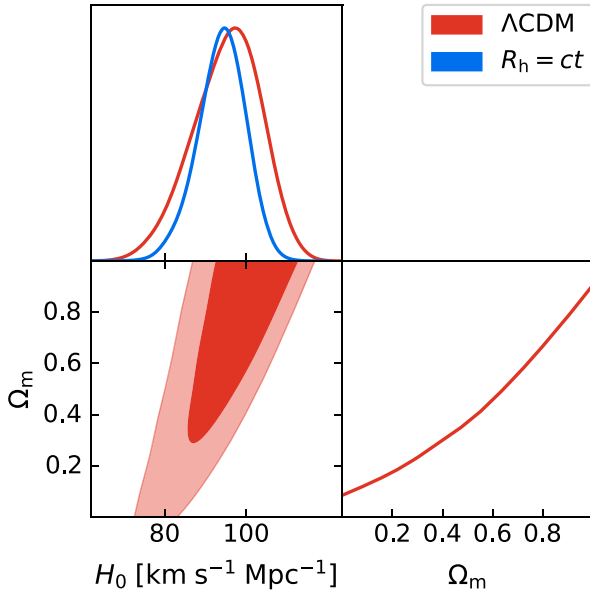


Figure 2. 1D marginalized posterior distributions and 2D 1–2 σ contour regions representing the cosmological parameters H_0 and/or Ω_m , constrained by 24 localized FRBs. The colours represent: flat Λ CDM (red contours) and $R_h = ct$ (blue line).

IGM baryon fraction f_{IGM} is fixed to be 0.83 (Fukugita et al. 1998). Moreover, there is a degeneracy between the Hubble constant H_0 and the baryon density parameter Ω_b in Equation (5), so we adopt a fixed value $\Omega_b = 0.0493$ for the sake of constraining H_0 (Planck Collaboration et al. 2020).

In flat Λ CDM, the dimensionless Hubble parameter ($H[z]/H_0$) is well approximated by

$$E^{\Lambda\text{CDM}}(z) = [\Omega_m(1+z)^3 + \Omega_\Lambda]^{1/2}, \quad (9)$$

where Ω_m is the present-day scaled matter energy density and $\Omega_\Lambda = 1 - \Omega_m$ is the vacuum energy density (assuming spatial flatness). We allow Ω_m to vary. In this model, the free parameters are thus H_0 and Ω_m .

On the other hand, the dimensionless expansion rate in the $R_h = ct$ universe (Melia 2007; Melia & Shevchuk 2012; Melia 2020), is given as

$$E^{R_h=ct}(z) = 1 + z. \quad (10)$$

In this model, we have only one free parameter that need to be optimized: H_0 .

For each model, we use the Python Markov chain Monte Carlo (MCMC) module, EMCEE (Foreman-Mackey et al. 2013), to explore the posterior probability distributions of the free parameters. In our MCMC analysis, we set wide flat priors on $H_0 \in [0, 150]$ km s $^{-1}$ Mpc $^{-1}$ and/or $\Omega_m \in [0, 1]$. The 1D marginalized posterior distributions and 2D plots of the 1–2 σ confidence regions for these parameters, constrained

by 24 localized FRBs, are displayed in Figure 2. For Λ CDM, these red contours show that at the 1 σ confidence level, the inferred value is $H_0 = 95.8_{-9.2}^{+7.8}$ km s $^{-1}$ Mpc $^{-1}$, but that Ω_m is poorly constrained. Because the prior on Ω_m is uniform over the interval $[0, 1]$, only a median value of ~ 0.66 can be estimated. The maximum value of the likelihood function for optimized flat Λ CDM is given by $-2\ln\mathcal{L} = 308.97$, which will be used when comparing models using information criteria.

Given the high uncertainty in $\text{DM}_{\text{halo}}^{\text{MW}}$, here we set a wide flat prior $\text{DM}_{\text{halo}}^{\text{MW}} \in [5, 80]$ pc cm $^{-3}$. Taking a larger value of $\text{DM}_{\text{halo}}^{\text{MW}}$ will lead to a smaller value of DM_{IGM} , thus yielding a lower value of H_0 . Based on the estimate of Prochaska & Zheng (2019), we next consider whether a narrower flat prior $[50, 80]$ pc cm $^{-3}$ affects the H_0 measurement. For Λ CDM, we have also performed a parallel comparative analysis of the FRB data by marginalizing $\text{DM}_{\text{halo}}^{\text{MW}}$ over a flat prior of 50–80 pc cm $^{-3}$. In this case, the constraints on the cosmological parameters are $H_0 = 77.1_{-7.4}^{+7.0}$ km s $^{-1}$ Mpc $^{-1}$ and $\Omega_m \sim 0.56$. As expected, the adoption of a higher value of $\text{DM}_{\text{halo}}^{\text{MW}}$ leads to a lower H_0 measurement. It is obvious that the $\text{DM}_{\text{halo}}^{\text{MW}}$ prior has a significant impact on the H_0 measurement.

Even though the large H_0 ($95.8_{-9.2}^{+7.8}$ km s $^{-1}$ Mpc $^{-1}$) for the given flat prior of 5–80 pc cm $^{-3}$ is the result we obtain with the current best knowledge of $\text{DM}_{\text{halo}}^{\text{MW}}$, we want to point out some potential caveats to this measurement. (i) In general, an underestimated host contribution could be the most likely cause of an elevated H_0 . The probability density function for DM_{host} has limited theoretical motivation. We don’t know if $P_{\text{host}}(\text{DM}_{\text{host}})$ can represent the shape of the host contribution well, and as we have already noticed, there are bursts like FRB 20190520B with a large DM_{host} contribution. (ii) The effect of observational biases against high-DM FRBs might be the other cause of an elevated H_0 . Here we use the $\text{DM}-z$ relation of localized FRBs to constrain H_0 . However, at very high DMs, only nearby FRBs are detectable, since an event must be observed with sufficiently high fluence to overcome the detection bias against high DM. That is, observational biases cause the $\text{DM}-z$ relation to become inverted (James et al. 2022a). More localized FRBs will be necessary to quantitatively estimate this effect.

Given the wide flat prior $\text{DM}_{\text{halo}}^{\text{MW}} \in [5, 80]$ pc cm $^{-3}$, the results of fitting the 24 $\text{DM}_{\text{obs}}-\text{redshift}$ data with the $R_h = ct$ universe are shown as the blue line in Figure 2. We have $H_0 = 94.2_{-6.2}^{+5.6}$ km s $^{-1}$ Mpc $^{-1}$. For the optimized $R_h = ct$ fit, the maximum value of the likelihood function yields $-2\ln\mathcal{L} = 310.18$.

To assess how these two models compare with each other, we show in Figure 1 the expected relations between DM_{IGM} and redshift for Λ CDM (with the best-fitting parameters $H_0 = 95.8$ km s $^{-1}$ Mpc $^{-1}$ and $\Omega_m = 0.66$; solid line) and for $R_h = ct$

(with $H_0 = 94.2 \text{ km s}^{-1} \text{ Mpc}^{-1}$; dashed line). One can see from this plot that the differences between alternative cosmological models emerge more prominently at higher redshifts.

Since these two models have different numbers of free parameters, however, a comparison of the likelihoods judging which cosmology is a better match to the data must be based on model selection tools. One tool commonly used to differentiate between cosmological models is the Bayesian Information Criterion (BIC; Schwarz 1978),

$$\text{BIC} = -2 \ln \mathcal{L} + (\ln N) f, \quad (11)$$

where N is the number of data points (here 24) and f is the number of free parameters (four for ΛCDM and three for $R_h = ct$). With BIC_α characterizing model \mathcal{M}_α , the unnormalized confidence that this model is true is the Bayesian weight $\exp(-\text{BIC}_\alpha/2)$. The likelihood of model \mathcal{M}_α being correct relative to the other one is then

$$P(\mathcal{M}_\alpha) = \frac{\exp(-\text{BIC}_\alpha/2)}{\exp(-\text{BIC}_1/2) + \exp(-\text{BIC}_2/2)}. \quad (12)$$

The model with the smaller BIC score is evidently preferred by this criterion. Our analysis shows that $R_h = ct$ is favored over ΛCDM with a likelihood of $\sim 73\%$ versus $\sim 27\%$.

4. MONTE CARLO SIMULATIONS

Though $R_h = ct$ is somewhat favored by this analysis, it is obvious that the current sample of FRBs is too small to differentiate strongly between this model and standard ΛCDM . To forecast how many localized FRBs are required to really distinguish the models, we shall here produce mock samples of FRBs through Monte Carlo simulations. In using the BIC model selection tool, the difference $\Delta\text{BIC} \equiv \text{BIC}_1 - \text{BIC}_2$ determines the extent to which model \mathcal{M}_1 is favored over \mathcal{M}_2 . The outcome of the difference is judged ‘positive’ in the range $\Delta\text{BIC} = 2 - 6$, ‘strong’ for $\Delta\text{BIC} = 6 - 10$, and ‘very strong’ for $\Delta\text{BIC} > 10$. In this section, we shall provide a quantitative assessment of how many FRB detections are necessary to rule out $R_h = ct$ or ΛCDM , by conservatively seeking an outcome even beyond $\Delta\text{BIC} \simeq 11.62$. That is, we shall consider two cases: one in which the background cosmological model is assumed to be ΛCDM , and the other in which it is $R_h = ct$, and we shall estimate the number of FRBs required in each case to rule out the alternative model with a likelihood $\sim 99.7\%$ versus $\sim 0.3\%$, corresponding to a 3σ confidence level.

The simulated FRBs are each characterized by the parameters $(z, \text{DM}_{\text{ext}})$. The procedures of simulation are as follows:

1. We assume that FRBs and gamma-ray bursts have the similar redshift distribution (Shao et al. 2011; Zhou et al. 2014), which is estimated as $P(z) \propto ze^{-z}$. The redshift z of our synthetic FRBs is generated randomly from this distribution in the redshift range $0 < z < 3$.

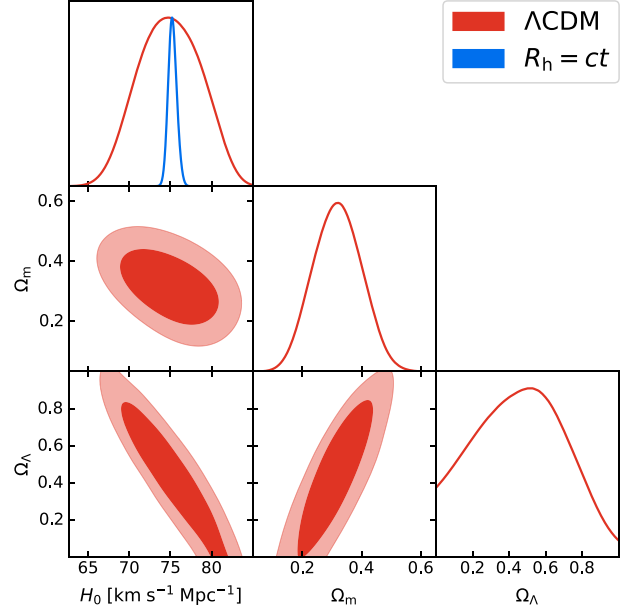


Figure 3. 1D marginalized posterior distributions and 2D $1-2\sigma$ contour regions for the cosmological parameters H_0 , Ω_m , and/or Ω_Λ , using the simulated sample with 1,150 FRBs, assuming ΛCDM as the background cosmology. The colours represent: the best-fit non-flat ΛCDM (red contours) and $R_h = ct$ (blue line).

2. With the mock z , DM_{host} is generated randomly from the probability distribution in Equation (4).
3. With the mock z , we infer the mean value $\langle \text{DM}_{\text{IGM}}(z) \rangle$ from Equation (5) corresponding either to a flat ΛCDM cosmology with $\Omega_m = 0.315$ and $H_0 = 67.4 \text{ km s}^{-1} \text{ Mpc}^{-1}$ (Section 4.1), or the $R_h = ct$ universe with $H_0 = 67.4 \text{ km s}^{-1} \text{ Mpc}^{-1}$ (Section 4.2).
4. With the selected z and $\langle \text{DM}_{\text{IGM}}(z) \rangle$, DM_{IGM} is generated randomly from the probability distribution in Equation (6).
5. With the mock DM_{host} and DM_{IGM} , we calculate DM_{ext} according to Equation (2).

For a mock FRB sample with a fixed number N , we optimize the model fits using the analysis method described in the previous section. To ensure the final results are unbiased, we repeat this process 100 times for a fixed number N of FRBs by using different noise seeds. The mock FRB sample is enlarged until the likelihood criterion discussed above is reached.

4.1. Assuming ΛCDM as the Background Cosmology

In the first case, we assume that the background cosmological model is ΛCDM , and seek the minimum sample size required to rule out $R_h = ct$ at the 3σ confidence level. We

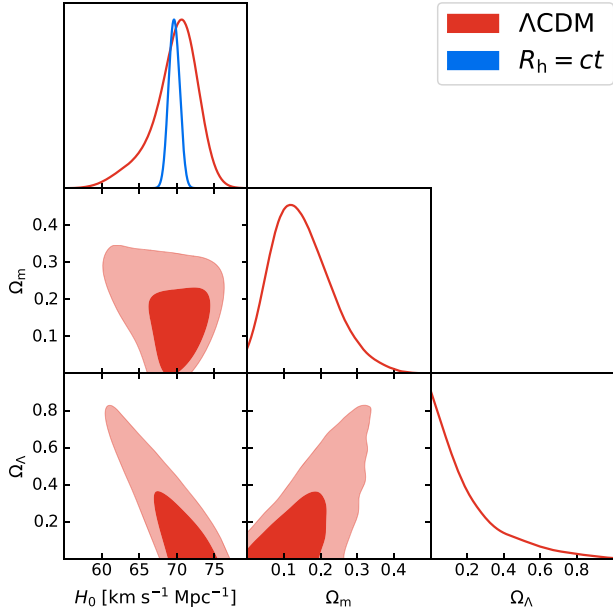


Figure 4. Same as Figure 3, except now using the simulated sample with 550 FRBs, assuming $R_h = ct$ as the background cosmology.

have found that a sample of at least 1,150 FRBs is necessary to achieve this goal. The best-fit parameters corresponding to the Λ CDM model for these simulated FRBs are displayed as red contours in Figure 3. To allow for greater flexibility in this fit, we relax the assumption on flatness, and allow Ω_Λ to be a free parameter, along with Ω_m . In non-flat Λ CDM, the dimensionless Hubble parameter is given by $E^{\Lambda\text{CDM}}(z) = [\Omega_m(1+z)^3 + \Omega_\Lambda + \Omega_k(1+z)^2]^{1/2}$, where $\Omega_k = 1 - \Omega_m - \Omega_\Lambda$ is the spatial curvature of the Universe. The best-fit values for Λ CDM using the simulated sample with 1,150 FRBs are $H_0 = 74.8^{+4.1}_{-3.9}$ km s⁻¹ Mpc⁻¹, $\Omega_m = 0.32^{+0.08}_{-0.08}$, and $\Omega_\Lambda = 0.46^{+0.25}_{-0.27}$.

In Figure 3, we also show the corresponding 1D posterior distribution of H_0 for the $R_h = ct$ universe (see the blue line). The best-fit value for the simulated sample is $H_0 = 75.2^{+0.5}_{-0.5}$ km s⁻¹ Mpc⁻¹. With $N = 1,150$, our analysis shows that the BIC would favor non-flat Λ CDM over $R_h = ct$ by an overwhelming likelihood of 99.7% versus only 0.3% (i.e., the prescribed 3σ confidence level).

4.2. Assuming $R_h = ct$ as the Background Cosmology

Assuming $R_h = ct$ as the background cosmology, we have found that a minimum of 550 FRBs are required to rule out the non-flat Λ CDM model. The 1D marginalized posterior distributions and 2D plots of the $1-2\sigma$ confidence regions for two-parameter combinations, constrained by 550 simulated FRBs are displayed in Figure 4. For non-flat Λ CDM, these red contours show that at the 1σ confidence level, the inferred values are $H_0 = 70.1^{+2.4}_{-3.4}$ km s⁻¹ Mpc⁻¹ and $\Omega_m = 0.14^{+0.09}_{-0.07}$, but

that Ω_Λ is poorly constrained; only an upper limits of < 0.24 can be estimated.

The corresponding 1D posterior distribution of H_0 for the $R_h = ct$ universe is shown as the blue line in Figure 4. The best-fit value for the simulated sample with 550 FRBs is $H_0 = 69.6^{+0.7}_{-0.7}$ km s⁻¹ Mpc⁻¹. With $N = 550$, our analysis shows that in this case the BIC would favor $R_h = ct$ over non-flat Λ CDM by an overwhelming likelihood of 99.7% versus only 0.3% (i.e., the prescribed 3σ confidence level).

5. INVESTIGATING THE HUBBLE TENSION

The $\text{DM}_{\text{IGM}}-z$ relation of FRBs has been used to probe cosmology, but this approach is limited by the poorly constrained dispersion measure, DM_{host} , contributed by the host galaxy (Macquart et al. 2020). Most of the previous work has been carried out by assuming a significant positive skew for the distribution of DM_{host} and/or DM_{IGM} , including the treatment described in Section 3. Here, we present a straightforward method of deriving an upper limit to H_0 without having to make any assumption regarding the probability distribution for DM_{host} .

Equation (5) shows that the theoretical DM_{IGM} at any given redshift is proportional to H_0 . An upper limit for H_0 can therefore be obtained by requiring that DM_{ext} (derived from Eq. 2) be at least as large as DM_{IGM} at the corresponding redshifts. In other words, DM_{ext} can be used to derive an upper limit to DM_{IGM} , and thus an average upper limit³ for H_0 , without the inclusion of the poorly known DM_{host} . In addition, $\text{DM}_{\text{halo}}^{\text{MW}}$ in Equation (2) is also uncertain. Its inclusion would yield a more stringent upper limit on H_0 . To be as conservative as possible, we therefore avoid introducing $\text{DM}_{\text{halo}}^{\text{MW}}$ in Equation (2). Hereafter, we thus conservatively constrain H_0 using the less restrictive extragalactic dispersion measures $\text{DM}'_{\text{ext}} = \text{DM}_{\text{obs}} - \text{DM}_{\text{ISM}}^{\text{MW}}$. The method of placing an upper bound on H_0 was first developed by James et al. (2022b), though those authors fixed $\Omega_b h^2$ rather than Ω_b , thus producing a ‘lower’ bound. This approach results in DM_{ext} becoming negatively correlated with H_0 , hence producing a lower limit for H_0 rather than an upper limit.

Utilizing the observed data \mathbf{D} (with the ‘extragalactic’ dispersion measures at redshifts z_i taken to be $\text{DM}'_{\text{ext},i}$) and some prior knowledge about the hypothetical cosmological models (for which the parameters are denoted by the vector θ), the posterior distribution of the free parameters is modeled through the half-Gaussian (log-)likelihood (Vagnozzi et al.

³ Due to the large fluctuations in density, DM_{IGM} at a given redshift can vary by as much as 40% along different lines of sight at $z \sim 1$ (McQuinn 2014). In principle, the derived ‘upper limit’ may thus be exceeded for individual FRBs.

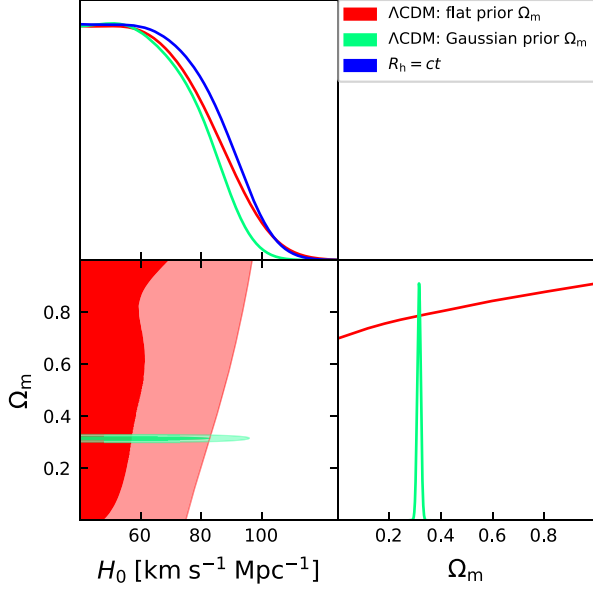


Figure 5. 1D marginalized posterior distributions and 2D 1–2 σ contour regions for H_0 and/or Ω_m . The colours represent: Λ CDM with a flat prior $\Omega_m \in [0, 1]$ (red), Λ CDM with a Gaussian prior $\Omega_m = 0.315 \pm 0.007$ (green), and $R_h = ct$ (blue).

2022; Wei & Melia 2022),

$$\ln \mathcal{L}(\boldsymbol{\theta} | \mathbf{D}) = -\frac{1}{2} \sum_i^{24} \begin{cases} \delta_i^2(\boldsymbol{\theta}) / \sigma_{\text{tot},i}^2 & \text{if } \delta_i(\boldsymbol{\theta}) < 0 \\ 0 & \text{if } \delta_i(\boldsymbol{\theta}) \geq 0, \end{cases} \quad (13)$$

where $\delta_i \equiv \text{DM}'_{\text{ext},i} - \langle \text{DM}_{\text{IGM}}(\boldsymbol{\theta}, z_i) \rangle$ and $\sigma_{\text{tot},i}^2 = \sigma_{\text{obs},i}^2 + \sigma_{\text{ISM}}^2 + \sigma_{\text{IGM}}^2(z_i)$. Here σ_{obs} , σ_{ISM} , and σ_{IGM} are the uncertainties associated with DM_{obs} , $\text{DM}_{\text{ISM}}^{\text{MW}}$, and the mean $\text{DM}_{\text{IGM}}(z)$, respectively. The Australia Telescope National Facility Pulsar Catalogue indicates that the average uncertainty in $\text{DM}_{\text{ISM}}^{\text{MW}}$ for sources at high Galactic latitude is about 10 pc cm^{-3} (Manchester et al. 2005), and we thus adopt this value for σ_{ISM} . Density fluctuations in the large-scale structure could lead to substantial sightline-to-sightline scatter around the mean $\text{DM}_{\text{IGM}}(z)$. Here we associate the standard deviation $\sigma_{\text{IGM}}(z)$ that results from the numerical simulation of McQuinn (2014) to $\text{DM}_{\text{IGM}}(z)$ (see their Fig. 1). Equation (13) expresses the fact that: *a*) since DM'_{ext} must not be smaller than the IGM portion, parameters for which DM'_{ext} is smaller than DM_{IGM} (i.e., $\delta_i(\boldsymbol{\theta}) < 0$) are exponentially unlikely, and this means the fit worsens as DM'_{ext} decreases relative to DM_{IGM} ; *b*) when DM'_{ext} is larger than DM_{IGM} (i.e., $\delta_i(\boldsymbol{\theta}) \geq 0$), the parameters are equally likely and cannot be differentiated on the basis of the FRB data alone.

For the flat Λ CDM model, the free parameters to be inferred in Equation (13) are $\boldsymbol{\theta} = \{H_0, \Omega_m\}$, for which we set flat priors: $H_0 \in [0, 150] \text{ km s}^{-1} \text{ Mpc}^{-1}$ and $\Omega_m \in [0, 1]$. The resulting constraints are displayed as red contours in Figure 5, which show that, whereas Ω_m is poorly constrained,

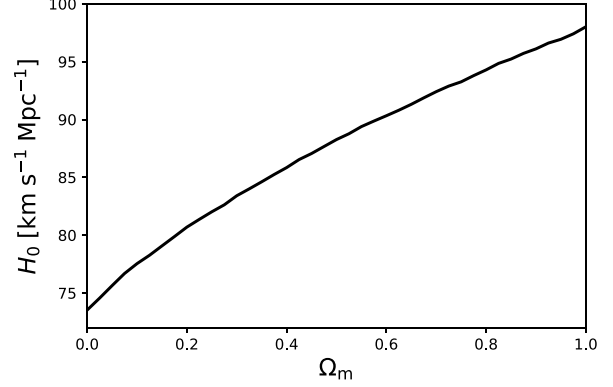


Figure 6. Inferred upper limit of H_0 as a function of Ω_m .

H_0 is assigned an upper limit, as expected. At the 95% confidence level, we find that $H_0 < 89.0 \text{ km s}^{-1} \text{ Mpc}^{-1}$ (the quoted upper limit corresponds to the 95th percentile of the posterior distribution of H_0). This upper limit is in good agreement with the latest local measurement ($73.04 \pm 1.04 \text{ km s}^{-1} \text{ Mpc}^{-1}$; Riess et al. 2022).

We carry this analysis further by investigating how the limit on H_0 is affected by the Ω_m prior. First, we assume a Gaussian prior $\Omega_m = 0.315 \pm 0.007$, informed by the *Planck* observations (Planck Collaboration et al. 2020). The green contours in Figure 5 show the joint H_0 – Ω_m posterior distributions obtained with the flat prior on H_0 and this Gaussian prior on Ω_m . In this case, the upper limit on the Hubble constant is $H_0 < 83.7 \text{ km s}^{-1} \text{ Mpc}^{-1}$. Next, we vary Ω_m over the range (0, 1). The inferred upper limit to H_0 is shown as a function of Ω_m in Figure 6.

Clearly, the upper limit to H_0 is very sensitive to the value of Ω_m . This echoes an interesting possibility proposed earlier (see, e.g., Melia 2015) that the disparity between the value of H_0 at high and low redshifts may in the end be due to a different emphasis placed on Ω_m by the CMB analysis versus its relevance to the local region. To find a best fit with Λ CDM, we need to optimize H_0 and Ω_m together, and Figure 6 shows that these parameters are tightly correlated. In other words, one could definitely argue that new physics would be needed if H_0 were the only quantity changing between high- z and low- z but, given this correlation, arising from a different emphasis being placed on Ω_m , the changing H_0 may just be due to a biasing of Ω_m at either high or low redshifts.

In the $R_h = ct$ cosmology, there is only one free parameter, i.e., $\boldsymbol{\theta} = \{H_0\}$. With the same flat prior on H_0 , we find an upper limit of $H_0 < 90.0 \text{ km s}^{-1} \text{ Mpc}^{-1}$ at the 95% confidence level (see the blue line in Figure 5), consistent with the value inferred from the local distance ladder. Again, the quoted upper limit corresponds to the 95th percentile of the posterior distribution of H_0 .

As shown in Section 3, if a wide flat prior, $DM_{\text{halo}}^{\text{MW}} \in [5, 80]$ pc cm^{-3} , is considered, we have $H_0 = 95.8_{-9.2}^{+7.8}$ $\text{km s}^{-1} \text{Mpc}^{-1}$ in our best fit analysis for ΛCDM . But in the analysis of deriving an upper limit to H_0 , we have $H_0 < 89.0$ $\text{km s}^{-1} \text{Mpc}^{-1}$ for ΛCDM . It seems strange that the best fit for ΛCDM requires a Hubble constant greater than the upper limit established at the 95% confidence level. This oddity is due to the fact that we use a different likelihood function (i.e., the half-Gaussian likelihood) for the upper limit analysis. Note that the optimized H_0 in our best fit analysis is also clearly not fully consistent with the estimate based on local distance measurements ($H_0 = 73.04 \pm 1.04$ $\text{km s}^{-1} \text{Mpc}^{-1}$; Riess et al. 2022) nor the value inferred from *Planck* ($H_0 = 67.4 \pm 0.5$ $\text{km s}^{-1} \text{Mpc}^{-1}$; Planck Collaboration et al. 2020). This may be an indication that our view of FRBs itself may be incomplete so that we don't fully understand how to interpret the observations yet. Nevertheless, if a narrower flat prior $DM_{\text{halo}}^{\text{MW}} \in [50, 80]$ pc cm^{-3} is adopted, we do get an optimized value of H_0 ($77.1_{-7.4}^{+7.0}$ $\text{km s}^{-1} \text{Mpc}^{-1}$) in line with our upper limit. It is easy to understand that the adoption of a larger value of $DM_{\text{halo}}^{\text{MW}}$ leads to a smaller value of DM_{IGM} , thus yielding a lower H_0 measurement.

6. SUMMARY AND DISCUSSION

As more and more FRBs have their DM_{IGM} associated with well-measured redshifts, they are emerging as potentially useful cosmic probes. In this work, we have affirmed the viability of using FRBs to constrain the low-redshift cosmic expansion and shed light on the growing Hubble tension.

We have used the dispersion measures of 24 localized FRBs within the redshift range $0.0337 \leq z \leq 1.016$ to compare the predictions of ΛCDM and $R_h = ct$. The free parameters of each model have been optimized via a maximization of the likelihood function. Given the wide flat prior $DM_{\text{halo}}^{\text{MW}} \in [5, 80]$ pc cm^{-3} , we have shown that flat ΛCDM fits the observations with $-2\ln\mathcal{L} = 308.97$, a Hubble constant $H_0 = 95.8_{-9.2}^{+7.8}$ $\text{km s}^{-1} \text{Mpc}^{-1}$ and $\Omega_m \sim 0.66$ (poorly constrained; only a median value can be estimated because the prior is uniform over the interval $[0, 1]$). One point worth emphasizing is that the H_0 measurement is affected dramatically by the $DM_{\text{halo}}^{\text{MW}}$ prior. For the same $DM_{\text{halo}}^{\text{MW}}$ prior, $R_h = ct$ fits these same data with $-2\ln\mathcal{L} = 310.18$, and a Hubble constant $H_0 = 94.2_{-6.2}^{+5.6}$ $\text{km s}^{-1} \text{Mpc}^{-1}$. Both models fit the data quite well. Flat ΛCDM has one additional free parameter compared to $R_h = ct$, however, so the latter is favored by the BIC with a likelihood of $\sim 73\%$ versus $\sim 27\%$.

This result is suggestive, though the current sample of FRBs is clearly too small for either model to be ruled out yet. We have therefore constructed two simulated samples in the redshift range $0 < z < 3$, one based on a ΛCDM background cosmology and the other built using $R_h = ct$. Through the analysis of these simulated FRBs, we have estimated that

a sample of at least 1,150 localized FRBs would be required to rule out $R_h = ct$ at a 3σ confidence level if the background cosmology is actually ΛCDM , while ~ 550 FRBs would be necessary to similarly rule out ΛCDM if the real cosmology is instead $R_h = ct$. The difference in required sample size is caused by ΛCDM 's larger number of free parameters and, therefore, a severe penalty from the BIC.

We have also adopted a straightforward method of deriving an upper limit to H_0 , eliminating possible biases due to the presumption of an unknown probability distribution of the DM contributed by the FRB host galaxy (DM_{host}). Owing to the theoretical IGM portion of DM (DM_{IGM}) being proportional to H_0 at any redshift, restricting DM_{ext} to be larger than the IGM portion it contains at any z delimits H_0 on the upside. Assuming flat ΛCDM , with a wide flat prior on Ω_m , we have obtained $H_0 < 89.0$ $\text{km s}^{-1} \text{Mpc}^{-1}$ at the 95% confidence level. The inferred upper limit to H_0 is very sensitive to Ω_m , however. The Hubble tension between the high- z and low- z measurements of H_0 may be due in part to the different emphasis placed on Ω_m by the CMB analysis versus its impact locally.

In the $R_h = ct$ cosmology, we found an upper limit of $H_0 < 90.0$ $\text{km s}^{-1} \text{Mpc}^{-1}$, also consistent with the low- z measurement. Our overall conclusion is that FRBs may become a powerful diagnostic to test the Hubble tension as their sample size grows with the accurate localization of future events.

Previously, within the context of ΛCDM , Hagstotz et al. (2022) (hereafter H22), James et al. (2022b) (hereafter J22), and Wu et al. (2022) (hereafter W22) used observations of FRBs to measure H_0 , finding $H_0 = 62.3 \pm 9.1$ $\text{km s}^{-1} \text{Mpc}^{-1}$, $H_0 = 73_{-8}^{+12}$ $\text{km s}^{-1} \text{Mpc}^{-1}$, and $H_0 = 68.8_{-4.3}^{+5.0}$ $\text{km s}^{-1} \text{Mpc}^{-1}$, respectively. These estimates are not fully consistent with our result of $H_0 = 95.8_{-9.2}^{+7.8}$ $\text{km s}^{-1} \text{Mpc}^{-1}$ at the 1σ confidence level. It is thus useful to compare differences in the analysis methods. For the analysis sample, H22, J22, and W22, respectively, used 9, 16 (including 60 unlocalized FRBs), and 18 localized FRBs to constrain H_0 , while our analysis focused on a larger sample of 24 localized FRBs.

For $DM_{\text{halo}}^{\text{MW}}$, J22 set a prior of 50 pc cm^{-3} , and W22 marginalized $DM_{\text{halo}}^{\text{MW}}$ using a Gaussian prior of $DM_{\text{halo}}^{\text{MW}} = 65 \pm 15$ pc cm^{-3} over the range of $[50, 80]$ pc cm^{-3} . Our work instead adopted a wide flat prior $DM_{\text{halo}}^{\text{MW}} \in [5, 80]$ pc cm^{-3} . Since their assumed $DM_{\text{halo}}^{\text{MW}}$ values are higher, their assumed DM_{IGM} will be decreased, which we assess to be the main reason for the lower H_0 values derived by J22 and W22. Note that if we used a narrower flat prior $DM_{\text{halo}}^{\text{MW}} \in [50, 80]$ pc cm^{-3} , our result of $H_0 = 77.1_{-7.4}^{+7.0}$ $\text{km s}^{-1} \text{Mpc}^{-1}$ would be in good agreement with previous estimates at the 1σ confidence level.

For the probability distributions of DM_{host} and DM_{IGM} , J22, W22, and our work used an asymmetric penalty to model them. H22 instead used a symmetric penalty for DM

lying away from the mean. They neither considered the asymmetric tail to large-DM values, nor the relatively sharp lower limit of DM at a given redshift expected for DM_{ext} . The inferred H_0 is very sensitive to the assumed value of the mean DM_{host} (or $\ln DM_{\text{host}}$). Moreover, numerical simulations show that the mean DM_{host} moderately increases with redshift. Neither H22 nor J22, however, considered the redshift evolution of DM_{host} . H22 assumed $\langle DM_{\text{host}} \rangle = 100 \text{ pc cm}^{-3}$ in a normal distribution, while J22 used a lognormal function for $\mu_{\text{host}} (\equiv \langle \ln DM_{\text{host}} \rangle)$, in which μ_{host} is treated as a constant free parameter. Following W22, we also used the same lognormal function to model μ_{host} based on the simulations of Zhang et al. (2020) with μ_{host} evolving with redshift, and varying according to the type of FRB host galaxy. Note that since the assumed value of $\langle DM_{\text{host}} \rangle$ in H22 is larger than our adopted $e^{\mu_{\text{host}}}$ values from the simulations of Zhang et al. (2020) and W22 did not include those FRBs with extreme values of DM_{obs} (such as FRBs 20190520B and 20210117A), their assumed DM_{IGM} will be decreased, which we view as the other reasons for the lower H_0 values derived by H22 and W22.

1 We would like to thank the anonymous referee for construc-
 2 tive comments that helped improve our work. We are also
 3 grateful to Prof. Fa-Yin Wang for sharing the $DM_{\text{IGM}}-z$ re-
 4 lation derived from the IllustrisTNG simulation with us. This
 5 work is partially supported by the National SKA Program
 6 of China (2022SKA0130100), the National Natural Science
 7 Foundation of China (grant No. 12041306), the Key Re-
 8 search Program of Frontier Sciences (grant No. ZDBS-LY-
 9 7014) of Chinese Academy of Sciences, International Part-
 10 nership Program of Chinese Academy of Sciences for Grand
 11 Challenges (114332KYSB20210018), the CAS Project for
 12 Young Scientists in Basic Research (grant No. YSBR-063),
 13 the CAS Organizational Scientific Research Platform for
 14 National Major Scientific and Technological Infrastructure:
 15 Cosmic Transients with FAST, the Natural Science Founda-
 16 tion of Jiangsu Province (grant No. BK20221562), and the
 17 Young Elite Scientists Sponsorship Program of Jiangsu As-
 18 sociation for Science and Technology.

REFERENCES

- Bannister, K. W., Deller, A. T., Phillips, C., et al. 2019, *Science*, 365, 565, doi: [10.1126/science.aaw5903](https://doi.org/10.1126/science.aaw5903)
- Becker, G. D., Bolton, J. S., Haehnelt, M. G., & Sargent, W. L. W. 2011, *MNRAS*, 410, 1096, doi: [10.1111/j.1365-2966.2010.17507.x](https://doi.org/10.1111/j.1365-2966.2010.17507.x)
- Bhandari, S., Sadler, E. M., Prochaska, J. X., et al. 2020, *ApJL*, 895, L37, doi: [10.3847/2041-8213/ab672e](https://doi.org/10.3847/2041-8213/ab672e)
- Bhandari, S., Heintz, K. E., Aggarwal, K., et al. 2022, *AJ*, 163, 69, doi: [10.3847/1538-3881/ac3aec](https://doi.org/10.3847/1538-3881/ac3aec)
- Bhardwaj, M., Kirichenko, A. Y., Michilli, D., et al. 2021a, *ApJL*, 919, L24, doi: [10.3847/2041-8213/ac223b](https://doi.org/10.3847/2041-8213/ac223b)
- Bhardwaj, M., Gaensler, B. M., Kaspi, V. M., et al. 2021b, *ApJL*, 910, L18, doi: [10.3847/2041-8213/abeaa6](https://doi.org/10.3847/2041-8213/abeaa6)
- Chatterjee, S., Law, C. J., Wharton, R. S., et al. 2017, *Nature*, 541, 58, doi: [10.1038/nature20797](https://doi.org/10.1038/nature20797)
- CHIME/FRB Collaboration, Amiri, M., Andersen, B. C., et al. 2021, *ApJS*, 257, 59, doi: [10.3847/1538-4365/ac33ab](https://doi.org/10.3847/1538-4365/ac33ab)
- Chittidi, J. S., Simha, S., Mannings, A., et al. 2021, *ApJ*, 922, 173, doi: [10.3847/1538-4357/ac2818](https://doi.org/10.3847/1538-4357/ac2818)
- Cordes, J. M., & Lazio, T. J. W. 2002, arXiv e-prints, astro. <https://arxiv.org/abs/astro-ph/0207156>
- Deng, W., & Zhang, B. 2014, *ApJL*, 783, L35, doi: [10.1088/2041-8205/783/2/L35](https://doi.org/10.1088/2041-8205/783/2/L35)
- Di Valentino, E., Mena, O., Pan, S., et al. 2021, *Classical and Quantum Gravity*, 38, 153001, doi: [10.1088/1361-6382/ac086d](https://doi.org/10.1088/1361-6382/ac086d)
- Foreman-Mackey, D., Hogg, D. W., Lang, D., & Goodman, J. 2013, *PASP*, 125, 306, doi: [10.1086/670067](https://doi.org/10.1086/670067)
- Fukugita, M., Hogan, C. J., & Peebles, P. J. E. 1998, *ApJ*, 503, 518, doi: [10.1086/306025](https://doi.org/10.1086/306025)
- Gao, H., Li, Z., & Zhang, B. 2014, *ApJ*, 788, 189, doi: [10.1088/0004-637X/788/2/189](https://doi.org/10.1088/0004-637X/788/2/189)
- Gao, R., Li, Z., & Gao, H. 2022, *MNRAS*, 516, 1977, doi: [10.1093/mnras/stac2270](https://doi.org/10.1093/mnras/stac2270)
- Hagstotz, S., Reischke, R., & Lilow, R. 2022, *MNRAS*, 511, 662, doi: [10.1093/mnras/stac077](https://doi.org/10.1093/mnras/stac077)
- Hashimoto, T., Goto, T., Lu, T.-Y., et al. 2021, *MNRAS*, 502, 2346, doi: [10.1093/mnras/stab186](https://doi.org/10.1093/mnras/stab186)
- Heintz, K. E., Prochaska, J. X., Simha, S., et al. 2020, *ApJ*, 903, 152, doi: [10.3847/1538-4357/abb6fb](https://doi.org/10.3847/1538-4357/abb6fb)
- Inoue, S. 2004, *MNRAS*, 348, 999, doi: [10.1111/j.1365-2966.2004.07359.x](https://doi.org/10.1111/j.1365-2966.2004.07359.x)
- Ioka, K. 2003, *ApJL*, 598, L79, doi: [10.1086/380598](https://doi.org/10.1086/380598)
- James, C. W., Prochaska, J. X., Macquart, J. P., et al. 2022a, *MNRAS*, 509, 4775, doi: [10.1093/mnras/stab3051](https://doi.org/10.1093/mnras/stab3051)
- James, C. W., Ghosh, E. M., Prochaska, J. X., et al. 2022b, *MNRAS*, 516, 4862, doi: [10.1093/mnras/stac2524](https://doi.org/10.1093/mnras/stac2524)
- Keating, L. C., & Pen, U.-L. 2020, *MNRAS*, 496, L106, doi: [10.1093/mnras/slaa095](https://doi.org/10.1093/mnras/slaa095)
- Kirsten, F., Marcote, B., Nimmo, K., et al. 2022, *Nature*, 602, 585, doi: [10.1038/s41586-021-04354-w](https://doi.org/10.1038/s41586-021-04354-w)
- Law, C. J., Butler, B. J., Prochaska, J. X., et al. 2020, *ApJ*, 899, 161, doi: [10.3847/1538-4357/aba4ac](https://doi.org/10.3847/1538-4357/aba4ac)
- Li, Z., Gao, H., Wei, J.-J., et al. 2019, *ApJ*, 876, 146, doi: [10.3847/1538-4357/ab18fe](https://doi.org/10.3847/1538-4357/ab18fe)

- Li, Z., Gao, H., Wei, J. J., et al. 2020, *MNRAS*, 496, L28, doi: [10.1093/mnras/laaa070](https://doi.org/10.1093/mnras/laaa070)
- Li, Z.-X., Gao, H., Ding, X.-H., Wang, G.-J., & Zhang, B. 2018, *Nature Communications*, 9, 3833, doi: [10.1038/s41467-018-06303-0](https://doi.org/10.1038/s41467-018-06303-0)
- Lorimer, D. R., Bailes, M., McLaughlin, M. A., Narkevic, D. J., & Crawford, F. 2007, *Science*, 318, 777, doi: [10.1126/science.1147532](https://doi.org/10.1126/science.1147532)
- Macquart, J. P., Prochaska, J. X., McQuinn, M., et al. 2020, *Nature*, 581, 391, doi: [10.1038/s41586-020-2300-2](https://doi.org/10.1038/s41586-020-2300-2)
- Manchester, R. N., Hobbs, G. B., Teoh, A., & Hobbs, M. 2005, *AJ*, 129, 1993, doi: [10.1086/428488](https://doi.org/10.1086/428488)
- Marcote, B., Nimmo, K., Hessels, J. W. T., et al. 2020, *Nature*, 577, 190, doi: [10.1038/s41586-019-1866-z](https://doi.org/10.1038/s41586-019-1866-z)
- McQuinn, M. 2014, *ApJL*, 780, L33, doi: [10.1088/2041-8205/780/2/L33](https://doi.org/10.1088/2041-8205/780/2/L33)
- Meiksin, A. A. 2009, *Reviews of Modern Physics*, 81, 1405, doi: [10.1103/RevModPhys.81.1405](https://doi.org/10.1103/RevModPhys.81.1405)
- Melia, F. 2007, *MNRAS*, 382, 1917, doi: [10.1111/j.1365-2966.2007.12499.x](https://doi.org/10.1111/j.1365-2966.2007.12499.x)
- . 2015, *Ap&SS*, 356, 393, doi: [10.1007/s10509-014-2211-5](https://doi.org/10.1007/s10509-014-2211-5)
- . 2020, *The Cosmic Spacetime* (Oxford: Taylor & Francis), doi: <https://doi.org/10.1201/9781003081029>
- . 2022, *PASP*, 134, 121001, doi: [10.1088/1538-3873/aca51f](https://doi.org/10.1088/1538-3873/aca51f)
- Melia, F., & Shevchuk, A. S. H. 2012, *MNRAS*, 419, 2579, doi: [10.1111/j.1365-2966.2011.19906.x](https://doi.org/10.1111/j.1365-2966.2011.19906.x)
- Muñoz, J. B., Kovetz, E. D., Dai, L., & Kamionkowski, M. 2016, *PhRvL*, 117, 091301, doi: [10.1103/PhysRevLett.117.091301](https://doi.org/10.1103/PhysRevLett.117.091301)
- Niu, C. H., Aggarwal, K., Li, D., et al. 2022, *Nature*, 606, 873, doi: [10.1038/s41586-022-04755-5](https://doi.org/10.1038/s41586-022-04755-5)
- Petroff, E., Hessels, J. W. T., & Lorimer, D. R. 2019, *A&A Rv*, 27, 4, doi: [10.1007/s00159-019-0116-6](https://doi.org/10.1007/s00159-019-0116-6)
- Planck Collaboration, Aghanim, N., Akrami, Y., et al. 2020, *A&A*, 641, A6, doi: [10.1051/0004-6361/201833910](https://doi.org/10.1051/0004-6361/201833910)
- Platts, E., Weltman, A., Walters, A., et al. 2019, *PhR*, 821, 1, doi: [10.1016/j.physrep.2019.06.003](https://doi.org/10.1016/j.physrep.2019.06.003)
- Prochaska, J. X., & Zheng, Y. 2019, *MNRAS*, 485, 648, doi: [10.1093/mnras/stz261](https://doi.org/10.1093/mnras/stz261)
- Prochaska, J. X., Macquart, J.-P., McQuinn, M., et al. 2019, *Science*, 366, 231, doi: [10.1126/science.aay0073](https://doi.org/10.1126/science.aay0073)
- Qiu, X.-W., Zhao, Z.-W., Wang, L.-F., Zhang, J.-F., & Zhang, X. 2022, *JCAP*, 2022, 006, doi: [10.1088/1475-7516/2022/02/006](https://doi.org/10.1088/1475-7516/2022/02/006)
- Ravi, V., Catha, M., D'Addario, L., et al. 2019, *Nature*, 572, 352, doi: [10.1038/s41586-019-1389-7](https://doi.org/10.1038/s41586-019-1389-7)
- Ravi, V., Law, C. J., Li, D., et al. 2022, *MNRAS*, 513, 982, doi: [10.1093/mnras/stac465](https://doi.org/10.1093/mnras/stac465)
- Riess, A. G., Yuan, W., Macri, L. M., et al. 2022, *ApJL*, 934, L7, doi: [10.3847/2041-8213/ac5c5b](https://doi.org/10.3847/2041-8213/ac5c5b)
- Ryder, S. D., Bannister, K. W., Bhandari, S., et al. 2022, *arXiv e-prints*, arXiv:2210.04680, doi: [10.48550/arXiv.2210.04680](https://doi.org/10.48550/arXiv.2210.04680)
- Schwarz, G. 1978, *Annals of Statistics*, 6, 461
- Shao, L., Dai, Z.-G., Fan, Y.-Z., et al. 2011, *ApJ*, 738, 19, doi: [10.1088/0004-637X/738/1/19](https://doi.org/10.1088/0004-637X/738/1/19)
- Thornton, D., Stappers, B., Bailes, M., et al. 2013, *Science*, 341, 53, doi: [10.1126/science.1236789](https://doi.org/10.1126/science.1236789)
- Vagnozzi, S. 2020, *PhRvD*, 102, 023518, doi: [10.1103/PhysRevD.102.023518](https://doi.org/10.1103/PhysRevD.102.023518)
- Vagnozzi, S., Pacucci, F., & Loeb, A. 2022, *Journal of High Energy Astrophysics*, 36, 27, doi: [10.1016/j.jheap.2022.07.004](https://doi.org/10.1016/j.jheap.2022.07.004)
- Verde, L., Treu, T., & Riess, A. G. 2019, *Nature Astronomy*, 3, 891, doi: [10.1038/s41550-019-0902-0](https://doi.org/10.1038/s41550-019-0902-0)
- Walters, A., Ma, Y.-Z., Sievers, J., & Weltman, A. 2019, *PhRvD*, 100, 103519, doi: [10.1103/PhysRevD.100.103519](https://doi.org/10.1103/PhysRevD.100.103519)
- Walters, A., Weltman, A., Gaensler, B. M., Ma, Y.-Z., & Witzemann, A. 2018, *ApJ*, 856, 65, doi: [10.3847/1538-4357/aaaf6b](https://doi.org/10.3847/1538-4357/aaaf6b)
- Wang, B., & Wei, J.-J. 2023, *ApJ*, 944, 50, doi: [10.3847/1538-4357/acb2c8](https://doi.org/10.3847/1538-4357/acb2c8)
- Wang, Y. K., & Wang, F. Y. 2018, *A&A*, 614, A50, doi: [10.1051/0004-6361/201731160](https://doi.org/10.1051/0004-6361/201731160)
- Wei, J.-J., Li, Z., Gao, H., & Wu, X.-F. 2019, *JCAP*, 2019, 039, doi: [10.1088/1475-7516/2019/09/039](https://doi.org/10.1088/1475-7516/2019/09/039)
- Wei, J.-J., & Melia, F. 2022, *ApJ*, 928, 165, doi: [10.3847/1538-4357/ac562c](https://doi.org/10.3847/1538-4357/ac562c)
- Wei, J.-J., Wu, X.-F., & Gao, H. 2018, *ApJL*, 860, L7, doi: [10.3847/2041-8213/aac8e2](https://doi.org/10.3847/2041-8213/aac8e2)
- Wu, Q., Zhang, G.-Q., & Wang, F.-Y. 2022, *MNRAS*, 515, L1, doi: [10.1093/mnras/slac022](https://doi.org/10.1093/mnras/slac022)
- Xiao, D., Wang, F., & Dai, Z. 2021, *Science China Physics, Mechanics, and Astronomy*, 64, 249501, doi: [10.1007/s11433-020-1661-7](https://doi.org/10.1007/s11433-020-1661-7)
- Xu, J., & Han, J. L. 2015, *Research in Astronomy and Astrophysics*, 15, 1629, doi: [10.1088/1674-4527/15/10/002](https://doi.org/10.1088/1674-4527/15/10/002)
- Yang, K. B., Wu, Q., & Wang, F. Y. 2022, *ApJL*, 940, L29, doi: [10.3847/2041-8213/aca145](https://doi.org/10.3847/2041-8213/aca145)
- Yu, H., & Wang, F. Y. 2017, *A&A*, 606, A3, doi: [10.1051/0004-6361/201731607](https://doi.org/10.1051/0004-6361/201731607)
- Zhang, B. 2022, *arXiv e-prints*, arXiv:2212.03972, <https://arxiv.org/abs/2212.03972>
- Zhang, G. Q., Yu, H., He, J. H., & Wang, F. Y. 2020, *ApJ*, 900, 170, doi: [10.3847/1538-4357/abaa4a](https://doi.org/10.3847/1538-4357/abaa4a)
- Zhang, L., & Li, Z. 2020, *ApJ*, 901, 130, doi: [10.3847/1538-4357/abb091](https://doi.org/10.3847/1538-4357/abb091)
- Zhang, Z. J., Yan, K., Li, C. M., Zhang, G. Q., & Wang, F. Y. 2021, *ApJ*, 906, 49, doi: [10.3847/1538-4357/abceb9](https://doi.org/10.3847/1538-4357/abceb9)
- Zhao, Z.-W., Li, Z.-X., Qi, J.-Z., et al. 2020, *ApJ*, 903, 83, doi: [10.3847/1538-4357/abb8ce](https://doi.org/10.3847/1538-4357/abb8ce)
- Zheng, Z., Ofek, E. O., Kulkarni, S. R., Neill, J. D., & Juric, M. 2014, *ApJ*, 797, 71, doi: [10.1088/0004-637X/797/1/71](https://doi.org/10.1088/0004-637X/797/1/71)

Zhou, B., Li, X., Wang, T., Fan, Y.-Z., & Wei, D.-M. 2014, *PhRvD*,
89, 107303, doi: [10.1103/PhysRevD.89.107303](https://doi.org/10.1103/PhysRevD.89.107303)